

1 Article

2 Experimental validation of a FSW model with an 3 enhanced friction law: application to a threaded 4 cylindrical pin tool

5 Narges Dialami ^{1,*}, Miguel Cervera ¹, Michele Chiumenti ¹,
6 Antonio Segatori ² and Wojciech Osikowicz ²

7 ¹ International Center for Numerical Methods in Engineering (CIMNE),
8 Universidad Polit cnica de Catalu a, Campus Norte UPC, 08034 Barcelona, Spain
9 e-mail: narges@cimne.upc.edu (N. Dialami), Miguel.Cervera@upc.edu (M. Cervera), michele@cimne.upc.edu
10 (M. Chiumenti),

11 ² Sapa AB Technology, Kanalгатan 1, 612 81 FINSP ANG, Sweden
12 Email: Antonio.Segatori@sapagroup.com (A. Segatori), Wojciech.Osikowicz@sapagroup.com (W. Osikowicz)

13 * Correspondence: narges@cimne.upc.edu

14 Academic Editor: name

15 Received: date; Accepted: date; Published: date

16 **Abstract:** This work adopts a fast and accurate two-stage computational strategy for the analysis of
17 FSW processes using threaded cylindrical pin tools. The coupled thermo-mechanical problem is
18 equipped with an enhanced friction model to include the effect of non-uniform pressure
19 distribution under the pin shoulder.

20 The overall numerical strategy is successfully validated by the experimental measurements
21 provided by the industrial partner (Sapa). The verification of the numerical model using the
22 experimental evidence is not only accomplished in terms of temperature evolution but also in
23 terms of torque, longitudinal, transversal and vertical forces.

24 **Keywords:** FSW; threaded pin; numerical model; experimental validation

25
26

27 1. Introduction

28 Friction Stir Welding (FSW) is a solid state joining technology in which friction and plastic dissipation are
29 sources of heat generation and material softening.

30 The tool pin profile has a remarkable effect on the friction between the tool and the workpiece and the foremost
31 effect on the plastic deformation of the surrounding material. FSW pin tools are often featured with thread
32 forms as they are beneficial for improving the tool performance and contribute to an effective material
33 transportation near the weld and the generation of a defect free stir zone [1].

34 Pin tools with threaded features are often used to investigate the relationship between the tool and the
35 microstructural properties obtained using different welding conditions.

36 In [2], thread pins are used for friction stir welding of two aluminium alloys: AA 7050-T7451 and AA 6061-T651.

37 They investigate the effect of the thread on the process in terms of in-plane reactions on the pin tool, torque,
38 temperature and the quality of welds.

39 In [1], the heat treatable AA 6061 and non-heat treatable AA 5086 aluminum alloys are welded by using three
40 different pin tools. It is found that FSW using threaded cylindrical pins provides better material flow between
41 two alloys among others.

42 In [3], the influence of the tool geometries upon the axial and translational forces, temperature and mechanical
43 properties for AA7075-T6 is studied. In their experimental work, the threaded tapered, non-threaded triangular
44 and non-threaded cylindrical pins are considered.

45 In [4], the effect of tool geometry on friction stir welding of polyethylene-polypropylene is investigated.
46 Threaded cylindrical, squared, triangular and straight cylindrical pin shapes are considered. Interaction effects
47 of welding variables, including rotational speed and traverse speed are studied.

48 In [5], a half-threaded pin tool to enhance the material flow at the lap interface is manufactured. The effect of
49 manufactured pin on the process is compared with that of full-threaded pin in terms of temperature, bonding
50 and material flow. It is observed, for instance, that the peak temperature during the process using the
51 half-threaded pin is lower than that using the full-threaded pin.

52 In [6], Colegrove et al. use the computational fluid dynamics (CFD) code, FLUENT, to model the 3D metal flow
53 in FSW using a threaded pin. It is found that the model generates an excessive amount of heat, leading to
54 over-prediction of the weld temperature.

55 Atharifar et al. [7], analyze the viscous and inertia loads applied to the FSW tool by varying the welding
56 parameters using FLUENT. A right-handed one-way thread pin tool with a concaved, smooth shoulder is
57 considered to simulate the material flow and heat transfer in the FSW of AA6061

58 Even though numerous studies, mainly experimental, of the effect of pin threads on the weld have been carried
59 out, there is an urgent need for a fast and accurate numerical model for the analysis of the FSW process. This
60 model should contain a suitable friction model to properly describe the tribological condition at the
61 tool/workpiece interface, capable of considering real process behavior such as the effect of non-uniform
62 pressure distribution under the tool.

63 A 3D finite element analysis is able to deal with several process complexities such as a concave shoulder, tool
64 tilt and threaded pin profiles. However, the large computational cost makes it inconceivable as a routinely used
65 design tool [8]. In previous works of the authors, a robust and fast numerical model was developed to study
66 FSW under different welding conditions [9-15]. A fully coupled thermo-mechanical model together with an
67 enhanced friction law was addressed to provide a more realistic thermo-mechanical response in comparison
68 with the existing models. The model took the benefits of an apropos kinematic framework combing Arbitrary
69 Lagrangian Eulerian (ALE), Eulerian and Lagrangian formulations for the stir zone, the workpiece and the
70 pin-tool, respectively. A two-stage speed-up strategy was incorporated to reduce the simulation time while
71 preserving the accuracy of the results.

72 In the present work, the model previously developed by the authors is adopted for the simulation of a FSW
73 process with a cylindrical threaded pin tool. The use of an apropos kinematic framework permits dealing with
74 arbitrary pin shapes as the threaded pin tool, without the necessity of using a re-meshing procedure due to the
75 large deformation of the material around the threaded pin tool. Moreover, it facilitates the application of the
76 boundary conditions. The enrichment of the model with an enhanced friction law permits to accurately predict
77 not only the temperature field but also the torque and forces exerted by the tool in all the directions. This is
78 mostly lacking in previous works in the FSW field. The use of a two-stage speed-up strategy is especially
79 important when simulating industrial cases, as the model is 3D and a large number of elements are used in the
80 discretization of the geometry. It is shown here that the framework, formulation and computational strategy are
81 not only applicable to featureless pins but also to pins with features such as threads. The analyses are calibrated

82 and validated through the experimental measurements performed by the industrial partner (Sapa) for
83 aluminum alloy Al6063-T6. The correlations obtained by means of this comparison not only validate the model
84 but also provide insight regarding the effects of the threaded pins upon torque, forces and temperature field.
85 Also, the differences between threaded and featureless cylindrical pins of similar dimensions are studied in
86 detail.

87 The paper is structured as follows: In the section 2, the overall solution strategy applied for simulation of FSW
88 process using cylindrical threaded pin tool is summarized. In section 3, the numerical assessment and the
89 calibration of the model using the experimental data are presented. Section 4 is devoted to the comparison of
90 the weld obtained using threaded and featureless cylindrical tool pins.

91

92 2. The solution strategy

93 In this work, a local analysis of the FSW process is performed. This means that the domain surrounding the
 94 Thermo-Mechanically Affected Zone (TMAZ) and the tool are considered in the simulation. The tool rotates
 95 rigidly with a constant speed and the plate moves with the advancing velocity opposite to the welding
 96 direction.

97 The governing equations and the boundary conditions used for the definition of the transient coupled
 98 thermo-mechanical problem are summarized in table 1. The nomenclature for the variables and properties
 99 involved is listed in table 2. Additional details on the formulation can be found in references [9] and [10].

100

101

Table 1. Balance and constitutive equations

Mechanical problem	
$\nabla \cdot \mathbf{s} + \nabla p + \rho_o \mathbf{b} = \mathbf{0}$	Momentum balance equation
$\nabla \cdot \mathbf{v} = 0$	Continuity equation
$\boldsymbol{\sigma} = p\mathbf{I} + \mathbf{s}$	Stress split
$\dot{\boldsymbol{\varepsilon}} = \nabla^s \mathbf{v}$	Kinematic equation
$\mathbf{s} = 2\mu_{eff}\dot{\boldsymbol{\varepsilon}}$	Constitutive equation
$\mu_{eff} = \mu(\sqrt{2\ \dot{\boldsymbol{\varepsilon}}\ })^{m-1}$	Norton-Hoff model
Thermal problem	
$\rho_0 c \left(\frac{1}{\alpha} \frac{dT}{dt} + (\mathbf{v} - \mathbf{v}_{mesh}) \cdot \nabla T \right) + \nabla \cdot \mathbf{q} = D_{mech}$	Energy balance equation
$\mathbf{q} = -k \nabla T$	Heat flux
$D_{mech} = \beta \mathbf{s} : \dot{\boldsymbol{\varepsilon}}$	Viscoplastic dissipation
$q_{conv} = h(T - T_{env})$	Heat convection
$q_{cond} = h_{cond}(T - T_{tool})$	Heat conduction

102

103

Table 2. Nomenclature

\mathbf{s}	Stress deviator
p	Pressure
ρ_0	density in the reference configuration
\mathbf{b}	body forces vector per unit of mass
\mathbf{v}	Velocity field
$\boldsymbol{\sigma}$	Cauchy's stress tensor
$\dot{\boldsymbol{\varepsilon}}$	Strain rate
μ_{eff}	Effective viscosity
μ	Viscosity parameter
m	Viscosity exponent
c	Specific heat
T	Temperature
\mathbf{v}_{mesh}	Velocity of the mesh
k	Thermal conductivity

β	Fraction of plastic dissipation converted into heat
h_{conv}	Heat transfer coefficient by convection
h_{cond}	Heat transfer coefficient by conduction
α	Speed-up factor
T_{env}	Environmental temperature
T_{tool}	Tool temperature

104

105 A two-stage simulation strategy is adopted [14]. A coupled thermo-mechanical problem is solved in both stages
106 ([13, 16]).

107 The first stage consists of a “forced” transient analysis aiming to reach the steady-state quickly. This objective is
108 achieved by increasing the thermal diffusivity in the energy balance equation. An acceleration parameter is
109 used to reduce the inertia term to speed-up this transient stage and reach the steady-state temperature field in a
110 decreased number of time-steps.

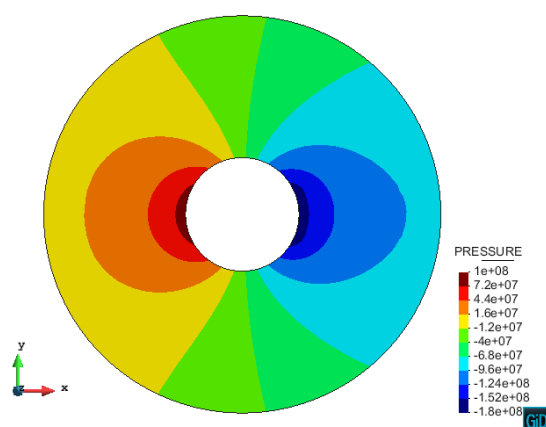
111 The second stage performs a transient analysis in which the temperature and velocity field obtained in the first
112 stage are considered as initial condition.

113 In the first stage, an Eulerian framework is adopted for the workpiece. Therefore, no periodic stage due to the
114 rotating movement of the tool is assumed. In the second stage, an apropos kinematic framework is adopted
115 taking advantage of combining ALE, Eulerian and Lagrangian formulations ([9], [10]). The Lagrangian
116 framework is used for the rotating pin, the ALE framework is considered at the stir zone of the work-piece
117 (TMAZ), and the Eulerian framework is used in the remaining part of the work-piece. This allows the analysis
118 of non-cylindrical pin shapes presenting the periodic solution due to the rotation of the tool.

119 The two-stage speed-up strategy performs the entire simulation preserving the capabilities of the original
120 model to predict FSW forces and torque for any types of pin shape in addition to the material flow visualization
121 [14].

122 Both plastic dissipation and friction are considered as the sources of heat generation. Friction is modelled by a
123 modified Norton’s friction model developed by authors in [15]. This model considers the effect of a
124 non-uniform pressure distribution under the tool (see figure 1 for a qualitative presentation of pressure
125 distribution around the tool) which results in higher friction in front of the tool and lower friction at the rear of
126 the tool.

127



128

129 **Figure 1.** Pressure distribution considering a fully slip contact condition (reproduced from [15])

130

131

132 The modified Norton's friction law reads:

$$\tau_T = a(x, T) \|\Delta \mathbf{v}_T\|^{q-1} \Delta \mathbf{v}_T = a(x, T) \|\Delta \mathbf{v}_T\|^q \mathbf{n} \quad (1)$$

133 where τ_T is the friction shear stress, $0 \leq q \leq 1$ is the sensitivity parameter and $\Delta \mathbf{v}_T$ is the relative sliding

134 velocity between the tool and the workpiece contact surfaces. $\mathbf{n} = \frac{\Delta \mathbf{v}_T}{\|\Delta \mathbf{v}_T\|}$ is the sliding direction. The

135 non-uniform consistency parameter $a(x, T)$ is defined by the following expression, to be considered at the

136 tool-workpiece interface, as:

$$a(x) = 0.5 \left(a_{\max} + a_{\min} + (a_{\max} - a_{\min}) \tanh \frac{x}{R/6} \right) \quad (2)$$

137 being x the position of each point located at the tool/workpiece interface, with respect to the rotation axis,
 138 projected along the welding direction and R the shoulder radius. Friction tractions vary from the maximum
 139 value at the front side of the shoulder to the minimum value at the rear side. Since the temperature in the
 140 working zone does not vary significantly, the maximum (a_{\max}) and minimum (a_{\min}) consistency parameters
 141 are assumed to be dependent on the average working temperature only.

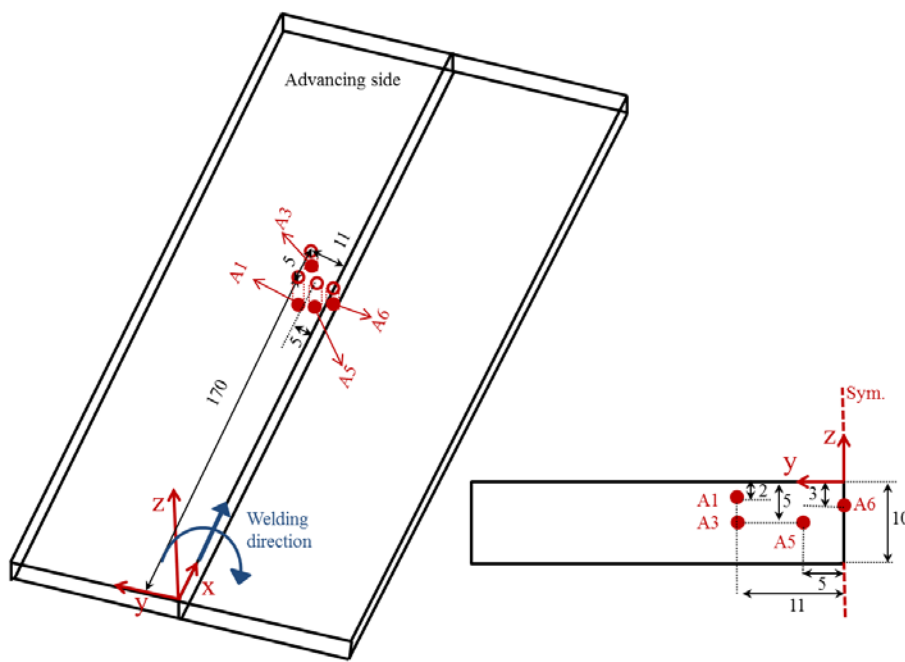
142

143 3. Validation of numerical model from experimental data

144 In this section, the numerical simulation of the FSW process is performed for a threaded pin tool. The results
 145 obtained using the modified Norton's friction model are compared with the experimental measurements
 146 performed by the industrial partner (Sapa).

147 The workpiece geometry is shown in figure 2 ($300 \times 50 \times 10 \text{ mm}^3$). The diameter of the tool shoulder is 18 mm. The
 148 average diameter and height of the tool pin are 7 mm and 4 mm, respectively. Figure 3 shows the experimental
 149 settings including the FSW robot, workpiece, tool, clamping system and thermocouples. The process
 150 parameters are: advancing velocity = 400 mm/minute and tool rotation speed = 600 rpm. The material used in
 151 this test is aluminium alloy (Al6063-T6). The temperature-dependent thermo-mechanical properties are shown
 152 in figure 4.

153 Figure 2 shows the position of the thermocouples in a transversal section of the workpiece with respect to the
 154 weld line. Their distance in mm with respect to a reference axis located at top left on the weld line is:
 155 A1(170,11,-5), A3(175,11,-2), A5(170,5,-5), A6(170,0,-3).



156

157

Figure 2. Workpiece geometry and the location of the thermocouples



158

Figure 3. Experimental setting and pin detail

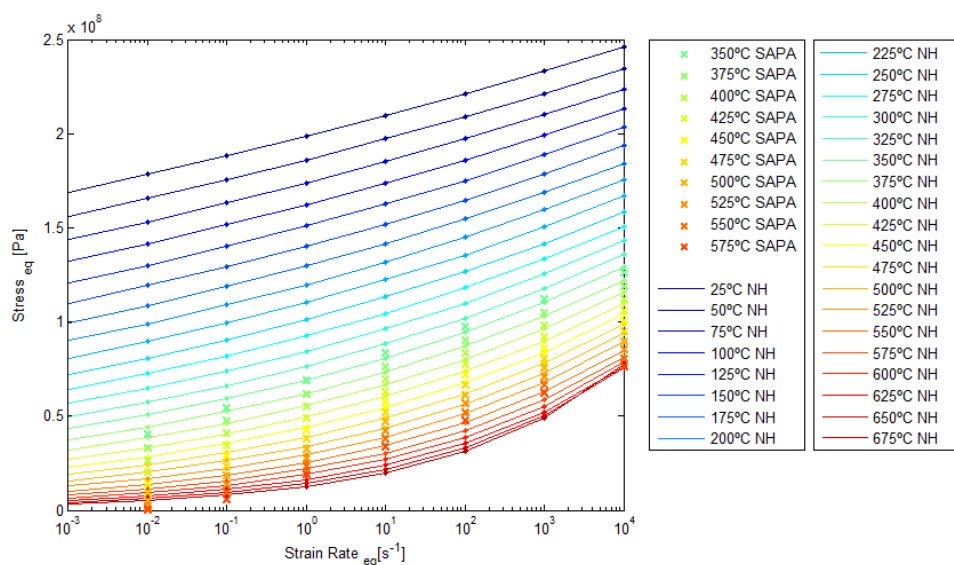


Figure 4. Material characterization

159

160

161

162 The simulation considers a domain of $50 \times 50 \times 10 \text{ mm}^3$. The tool advances in the x direction of the reference axes.
 163 It is assumed that 70 % of the plastic dissipation is converted into heat [17, 18].

164 Friction parameters a_{\min} and a_{\max} at the tool/workpiece interfaces (both pin and shoulder) are determined from
 165 the calibration of the friction model by matching the numerical results with the experimental data in terms of
 166 temperature evolution and process forces.

167 The analysis adopts $a_{\min} = 5 \times 10^7$ and $a_{\max} = 10^9$ at tool/workpiece interfaces. A vertical velocity of 2.4 mm/s is
 168 applied on the tool in order to obtain the vertical force exerted on the tool with the experiments.

169 The heat transfer coefficient, defining the heat loss by convection through the surrounding environment is:
 170 $h_{\text{conv}} = 10 \text{ W/m}^2\text{K}$ where the environment temperature is $T_{\text{env}} = 20^\circ\text{C}$.

171 The heat transfer coefficient by conduction (Newton's law) between the workpiece and the back-plate has been
 172 set to $h_{\text{cond}} = 2500 \text{ W/m}^2\text{K}$.

173 The values of heat loss by convection and conduction are obtained from series of calibration tests. The
 174 calibrated values are in the expected range. Typical values of heat transfer coefficients reported in the literature
 175 range from $h_{\text{cond}} = 350 \text{ W/m}^2\text{K}$ in Chao et al. [19] to $h_{\text{cond}} = 5,000 \text{ W/m}^2\text{K}$ in Khandkar et al. [20].

176 Note that radiation is an important heat loss mechanism at the Heat Affected Zone (HAZ), due to the high
 177 temperature field induced by the heat source. The radiation heat flux q_{rad} can be calculated using
 178 Stefan-Boltzmann's law: $q_{\text{rad}} = \sigma \epsilon (T^4 - T_{\text{env}}^4)$. The contribution of heat radiation can be also expressed as $q_{\text{rad}} = h_{\text{rad}}(T - T_{\text{env}})$; where $h_{\text{rad}}(T) = \sigma \epsilon (T^3 + T^2 T_{\text{env}} + T T_{\text{env}}^2 + T_{\text{env}}^3)$.

180 Heat is lost through the environment by a combination of convection and radiation. In practice, it is difficult to
 181 discriminate the effects of both heat transfer modes. For this reason, the numerical model assumes a combined
 182 heat transfer law, accounting for both heat convection and radiation: $q_{\text{conv}}(T) = h_{\text{conv}}(T - T_{\text{env}})$. In this case, q_{conv}
 183 represents the heat flux due to the simultaneous convection and radiation mechanisms, and h_{conv} is the
 184 corresponding equivalent heat transfer coefficient.

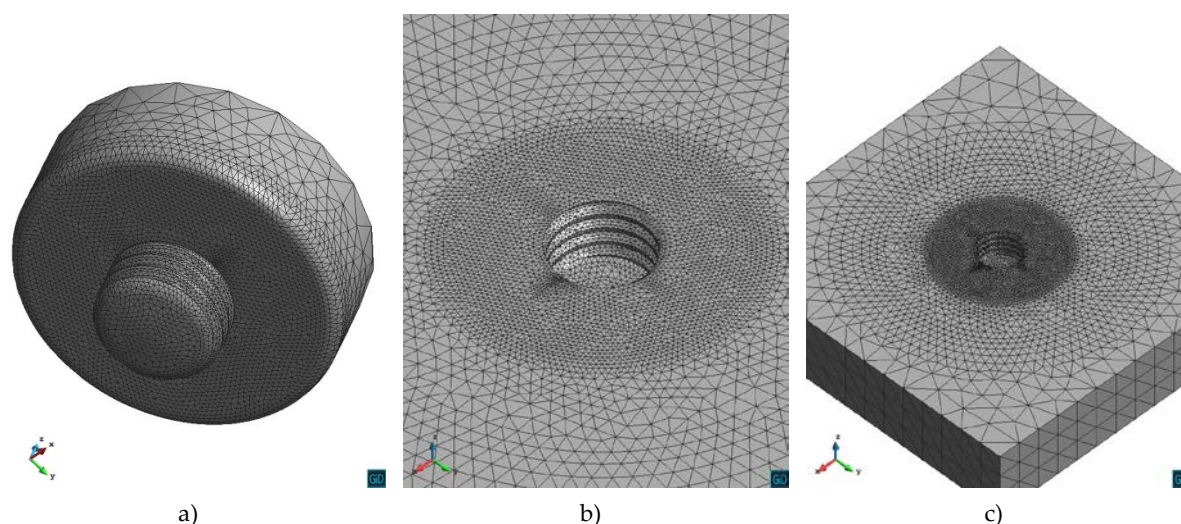
185 The mesh used in the simulation consists of 70,000 nodes and 400,000 tetrahedral elements. The mesh
 186 resolutions at the tool and the workpiece are shown in figure 5. A finer mesh is used in the vicinity of the
 187 pin-tool to capture the high temperature gradient in the TMAZ and to accurately define the geometry details.

188 In order to boost the convergence rate of this highly non-linear and coupled thermo-mechanical problem, a
 189 piecewise linearized Norton-Hoff model for different temperatures and strain rate values is assumed [14].

190 The agreement between the resulting values of torques, longitudinal, transversal and vertical forces obtained
 191 from the numerical model and the experimental measurements is significantly noticeable. Thanks to the friction
 192 model proposed by the authors, the overall numerical model is able to predict the transversal forces in
 193 agreement with the experimental data, while the commonly used friction laws such as Coulomb or Norton are
 194 incapable of capturing it [15]. In this work, the effect of the non-uniform pressure distribution below the tool
 195 translates into a non-uniform distribution of plastic dissipation, temperatures and friction tractions. This
 196 non-uniformity allows for the development of the transversal force up to the actual value recorded in the
 197 experimental measurements. Both experimental and numerical outcomes predict transversal forces higher than
 198 longitudinal forces.

199 Hence, the proposed framework for the numerical simulation of FSW process is capable of capturing accurately
 200 the mechanical results (Table 3). This also vouches for the robustness of our friction model proposed for the
 201 FSW.

202 The total processing time on an Intel core i7 processor is approximately 10 hours.
 203

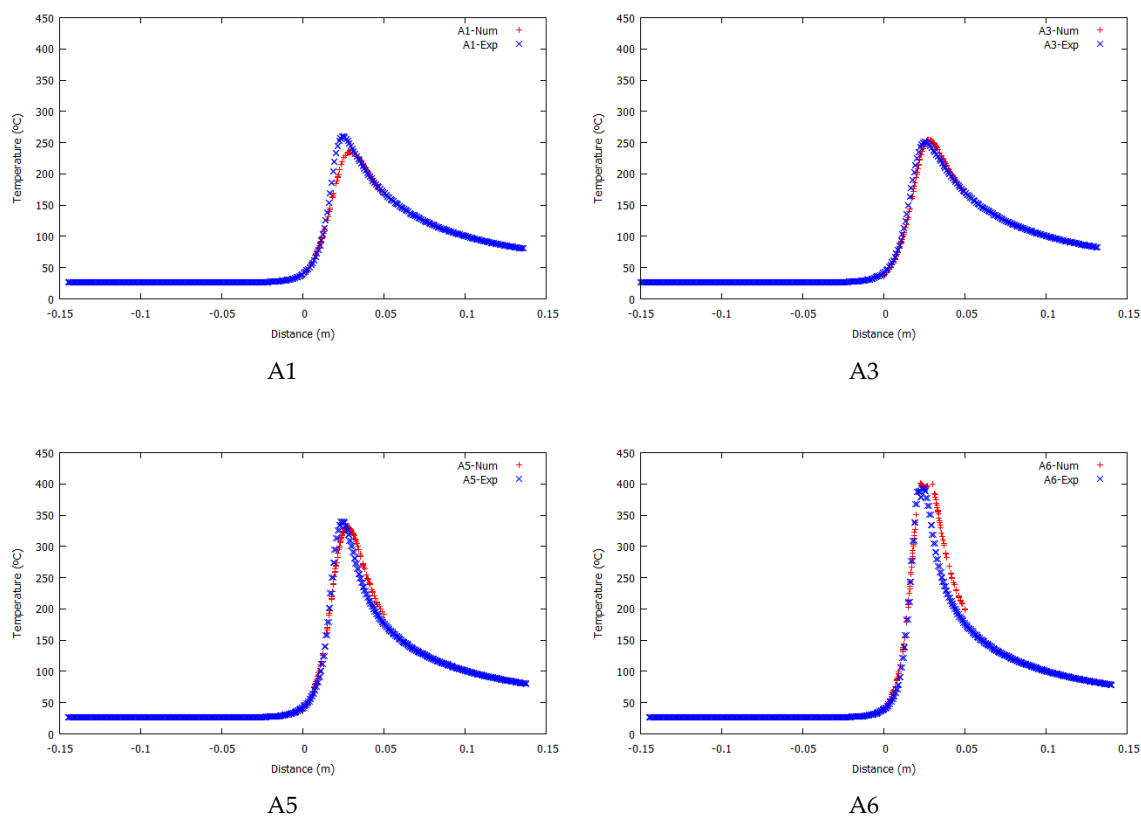


204 **Figure 5.** 3D tetrahedral mesh used: a) the tool; b) the workpiece (detail at the stir zone) and c) the workpiece
 205 (larger view).

206 **Table 3.** Forces and torque

$q=0.1$ $V_z=-0.0024$	Numerical model: $a_{max}=1e9$ $a_{min}=5e7$	Measurements: Sapa WT10
Torque (N.m)	64	62
Longitudinal force (N)	810	700
Transversal force (N)	1300	1000
Vertical force (N)	8200	8000

207



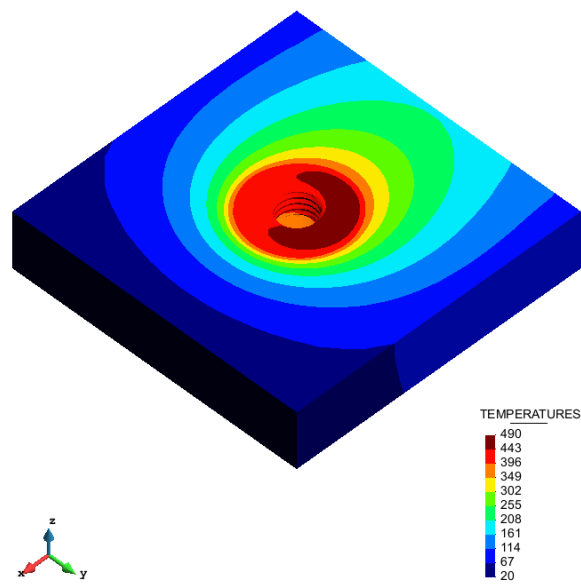
208

Figure 6. Temperature evolution in 4 thermocouples located in the workpiece

209 Figure 6 illustrates the temperature evolution at the four thermocouples located in the workpiece. In this figure,
 210 the comparison between numerical (Num) and experimental (Exp) results is presented. The response of the
 211 numerical model is found to be in a good agreement with the experimental measurements. Both experimental
 212 and numerical outcomes predict higher maximum temperature in the weld line decreasing with distance from
 213 the weld line and top surface.

214 In this work, the experimental data is provided at steady-state. Therefore, the transient simulation is performed
 215 until the (periodic) steady-state is reached. The maximum temperature recorded during the welding provides
 216 information indicating whether the process has attained the (periodic) steady-state [21, 22]. Under these
 217 conditions, the comparison between the temperature fields obtained from the numerical simulation and the
 218 experimental measurements is performed.

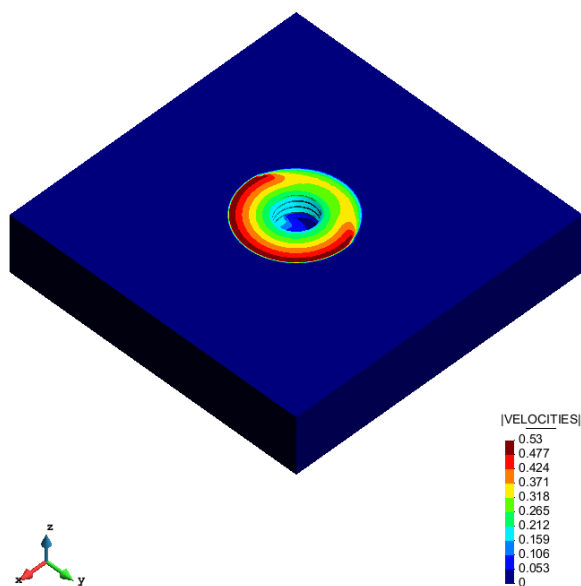
219 Figure 7 shows the temperature field at steady-state on the workpiece surface. The temperature distribution
 220 reveals a lower temperature at the head of the pin than the rear side. Thus, the flow stress is higher where the
 221 material is hotter. Figures 8 and 9 show the velocity and plastic dissipation contour fills computed from the
 222 numerical model. It can be clearly seen that the numerical model is able to represent the non-uniform
 223 distribution of the mentioned fields due to the use of the enhanced friction model. This non-uniformity results
 224 in the appearance of the transversal forces exerting on the tool.



225

226

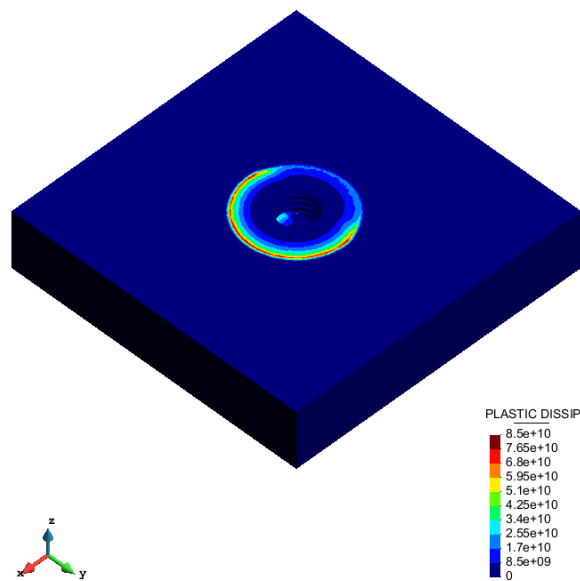
Figure 7. Temperature contour fills



227

228

Figure 8. Velocity contour fills



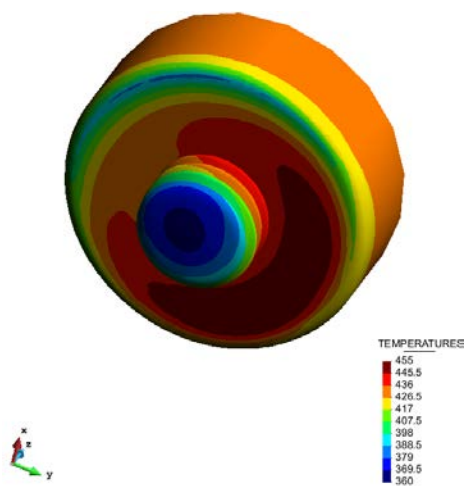
229

230

Figure 9. Plastic dissipation contour fills

231 The temperature contour fill on the tool surface is displayed in figure 10. Note that the temperature varies
232 between 360 °C and 455 °C. This shows that the temperature dependent parameters of the material and friction
233 models vary only within this range of temperature at the TMAZ.

234



235

236

Figure 10. Temperature distribution on the tool

237

238 4. FSW with featureless and threaded cylindrical pin

239 In this section, the thermo-mechanical results obtained for a featureless cylindrical pin (presented in [15]) are
 240 compared with the ones presented in the previous section for a threaded cylindrical pin. The comparison
 241 between these two cases is carried out after validating both simulations using threaded and featureless pins
 242 against the experimental measurements. The coupled thermo-mechanical model enriched with the enhanced
 243 friction model and the two-stage speed-up strategy used in both cases is identical. Thanks to the apropos
 244 kinematic framework adopted, the model can handle arbitrary pin shapes such as threaded profiles.

245 In both cases, the workpiece geometry, material properties and process parameters (advancing and rotating
 246 speed) are identical. The tool tilt angle is kept constant at 0° and the plunging depth of the pin-shoulder into the
 247 workpiece is negligible during the full welding process. The diameter and height of the featureless tool pin are
 248 7 mm and 4 mm, respectively.

249 The values $a_{\min}=4 \times 10^7$ and $a_{\max}=8 \times 10^8$ are used at tool/workpiece interfaces using the featureless tool while
 250 using threaded tool higher values of consistency parameters are used ($a_{\min}=5 \times 10^7$ and $a_{\max}=10^9$). The higher
 251 values of consistency parameters translate into an increase in the friction value which is consistent with the
 252 effect of the threads in a FSW process.

253 The vertical velocity is 2.5 mm/s in the case of featureless tool pins in order to obtain the applied vertical
 254 loading. It is slightly higher than the value applied for the threaded case.

255 The results for forces and torque using both types of tool profile are presented in table 4. Both cases present
 256 similar results, with lower values of forces and torque due to the thread effect, while maintaining a good
 257 agreement with the experimental measurements. A similar trend is also observed in reference [2] where the
 258 effects of pin features on material flow and friction stir weldability of two different aluminum
 259 alloys are studied. It is shown there that the featureless pin results in higher forces and torque than the threaded
 260 pin.

261

262 **Table 4.** Forces and torque (comparison between FSW process using threaded and featureless pin)

	Threaded pin		Featureless pin	
	Numerical model	Measurements	Numerical model	Measurements
Torque (N.m)	64	62	64	64
Longitudinal force (N)	810	700	870	500
Transversal force (N)	1300	1000	1700	1400
Vertical force (N)	8200	8000	8500	8200

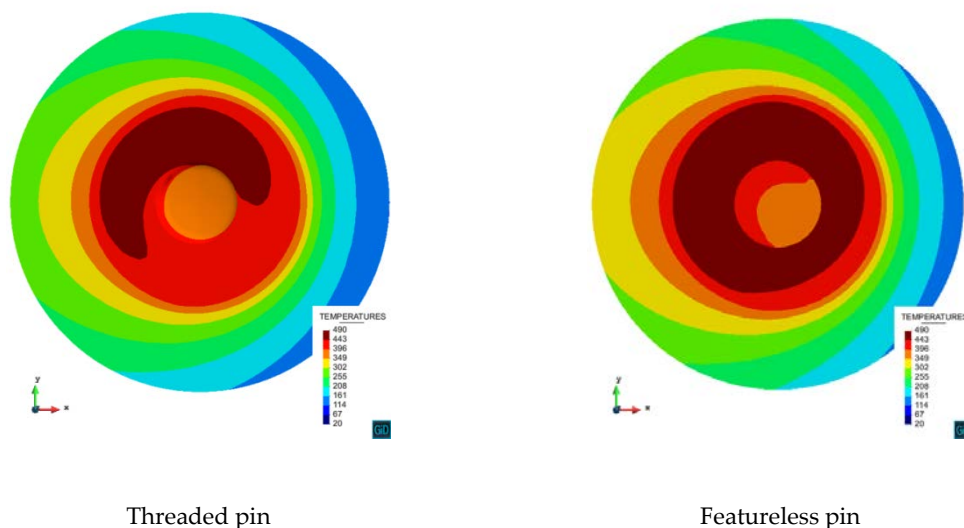
263

264 Figure 11 presents the temperature contours under the tool on the workpiece for both threaded and unthreaded
 265 tool pins. In the case of threaded pin, the difference in the temperature distribution on the retreating side and
 266 advancing side is more visible than in the unthreaded case. Hence, the friction model proposed is able to
 267 capture the non-uniformly distributed temperature around the tool.

268 The distribution of the plastic dissipation under the tool shoulder on the workpiece using both tool pins is
 269 compared in figure 12. The plastic dissipation is higher in front of the tool when using featureless pin and it is
 270 higher in the rear of the tool if threaded tool pin is considered.

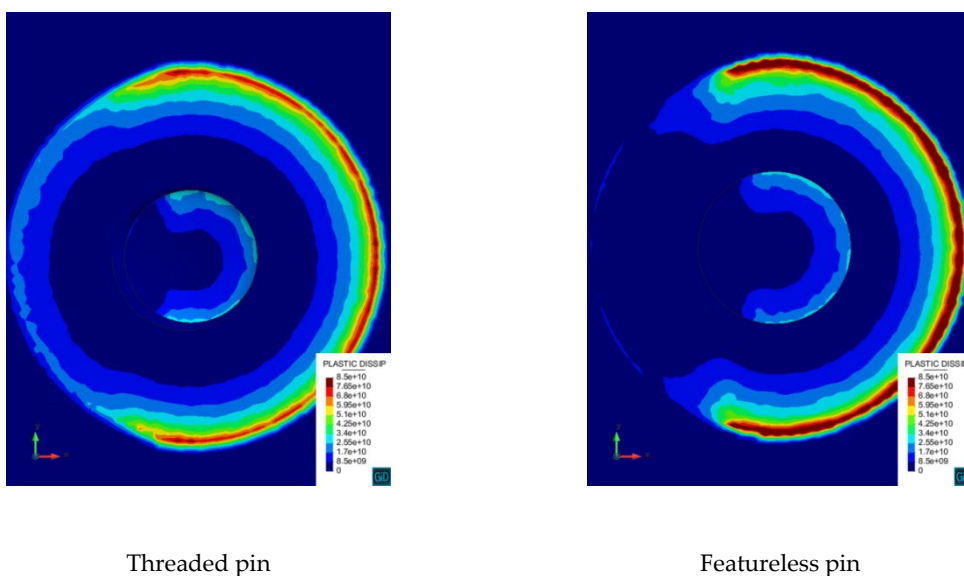
271 Figure 13 presents the velocity streamlines of three points located on a line 5 mm away from the rotation axis on
 272 the advancing side of both featureless and threaded pin tool and 2 mm away from the top surface. The
 273 differences observed in the streamlines show how the pin features affect the material movement. As expected,

274 the threaded pin increases the vertical movement. It is known that one of the threads effect on the FSW process
 275 is the increase in the vertical movement of the material around the pin [23]. Even without the threading, some
 276 amount of vertical material movement takes place. This was reported in [24] for a cylindrical unthreaded pin.
 277 The path of the two points which are not affected by the threaded pin movement passes around the featureless
 278 pin. Hence, separation of the streamlines on the advancing side around the featureless pin is observed.
 279
 280



281 **Figure 11.** Temperature distribution under the tool

282



283 **Figure 12.** Plastic dissipation contours under the tool

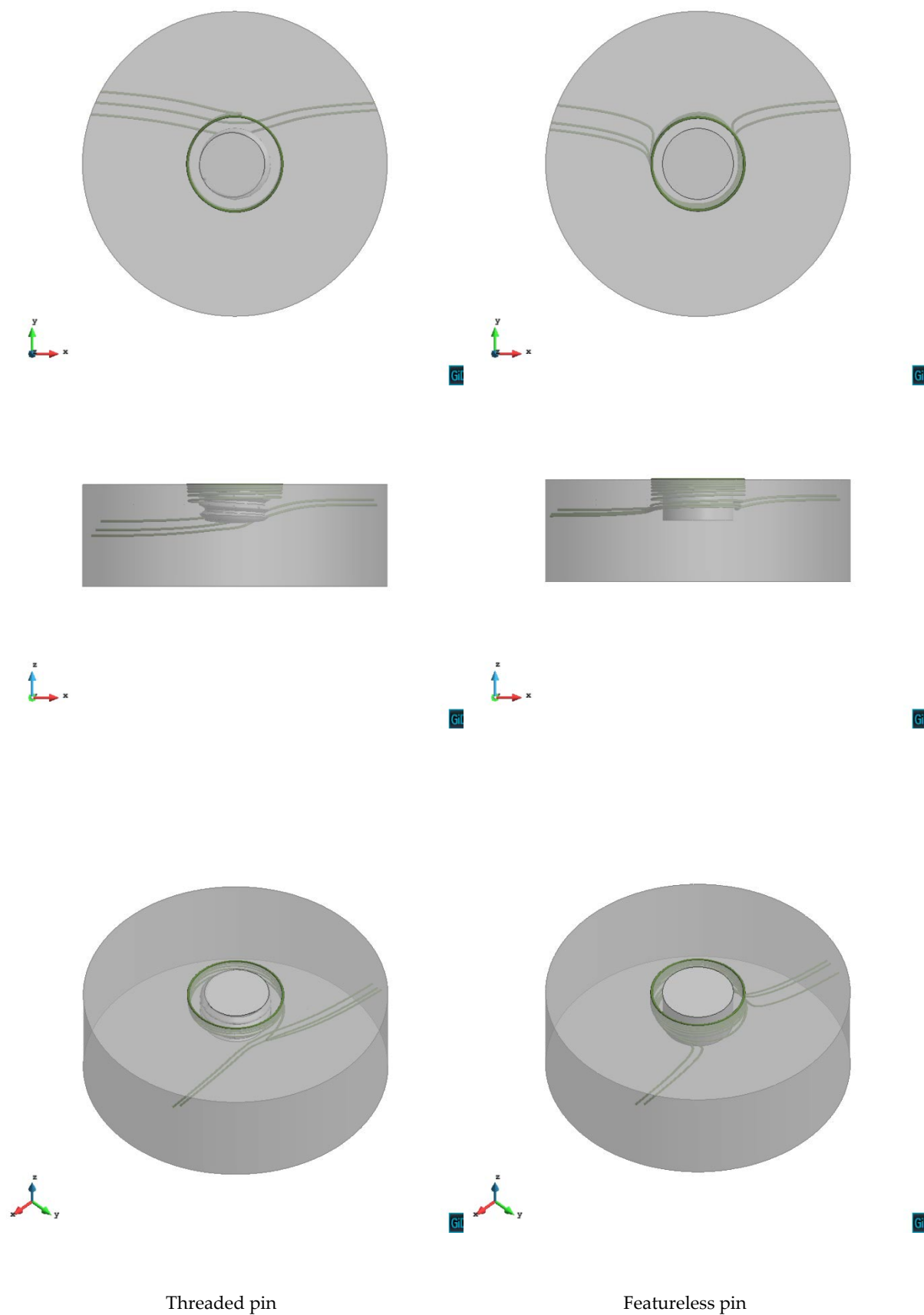


Figure 13. Velocity streamlines around the tool

285 5. Summary and conclusion

286 In this work, numerical simulations and the experimental calibration of a fast and accurate FEM model for FSW
287 analysis of a threaded cylindrical tool pin are presented. The main characteristics of the model are:

- 288 • Coupled thermo-mechanical scheme
- 289 • Simulation of arbitrary pin shapes
- 290 • Heat generation due to both friction and plastic dissipation
- 291 • Piecewise linear viscoplastic constitutive model
- 292 • Two-stage strategy for a significantly reduction of computational time
- 293 • Enhanced friction model accounting for the effect of non-uniform pressure distribution

294 The results of the FSW simulation using a threaded tool pin are presented in terms of longitudinal, transversal
295 and vertical forces, torque, as well as temperature distribution and compared with the experimental evidence.
296 The agreement between the numerical and experimental results, both in terms of thermal and mechanical
297 behaviours, is remarkable.

298 A comparison between the thermo-mechanical responses in FSW using threaded and featureless cylindrical
299 pins is also presented. Somewhat lower values of forces and torque are observed in case of threaded pin than
300 featureless one. The non-uniform distribution of heat generation around the tool using the enhanced friction
301 model is more visible in case of using a threaded pin. The threaded tool pin is found to increase the vertical
302 movement of the surrounding material.

303 It is shown that the proposed numerical model for the simulation of the FSW process is capable of capturing the
304 thermo-mechanical responses with remarkable accuracy for both the featureless and threaded pin tools.

305

306 **References**

- 307 1. Ilangovan M., Rajendra Boopathy S., Balasubramanian V., (2015) Effect of tool pin profile on
308 microstructure and tensile properties of friction stir welded dissimilar AA 6061–AA 5086 aluminium
309 alloy joints, *Defence Technology*, 11(2):174-184.
- 310 2. Reza-E-Rabby Md., Reynolds A. P. (2014) Effect of tool pin thread forms on friction stir weldability of
311 different aluminum alloys, *Procedia Engineering* 90: 637-642.
- 312 3. Papahn H., Bahemmat P., Haghpanahi M., Pour Aminaie I. (2015) Effect of friction stir welding tool
313 on temperature, applied forces and weld quality, *IET Science, Measurement & Technology*, 9(4) :
314 475-484.
- 315 4. Rezaee Hajideha M., Farahani M., Davoud Alavi S. A., Molla Ramezani N., (2017) Investigation on the
316 effects of tool geometry on the microstructure and the mechanical properties of dissimilar friction stir
317 welded polyethylene and polypropylene sheets, *Journal of Manufacturing Processes* 26:269–279.
- 318 5. Yu Z., Zhang W., Choo H., Feng Z.L., (2012) Transient heat and material flow modeling of friction
319 stir processing of magnesium alloy using threaded tool, *Metal Mater Trans A*, 43 (2): 724–737.
- 320 6. Colegrove P. A., Shercliff H. R., (2005) 3-Dimensional CFD modelling of flow round a threaded
321 friction stir welding tool profile, *Journal of Materials Processing Technology*, 169(2): 320-327.
- 322 7. Atharifar H., Lin D. and Kovacevic R. (2009) Numerical and Experimental Investigations on the Loads
323 Carried by the Tool During Friction Stir Welding, *Journal of Materials Engineering and Performance*
324 18:339–350.
- 325 8. Mishra R.S., Ma Z.Y. (2007) Friction stir welding and processing. ASM International, 2007 - Technology
326 & Engineering.
- 327 9. Chiumenti, M., Cervera, M., Agelet de Saracibar, C. and Dialami, N. (2012) Numerical modeling of
328 friction stir welding processes. *Computer Methods in Applied Mechanics and Engineering*,
329 254:353-369.
- 330 10. Dialami, N., Chiumenti, M., Cervera, M. and Agelet de Saracibar, C. (2013) An apropos kinematic
331 framework for the numerical modeling of friction stir welding. *Computers and Structures* 117:48-57.
- 332 11. Dialami N., Chiumenti M., Cervera M., Agelet de Saracibar C. and Ponthot J.-P. (2013) Material Flow
333 Visualization in Friction Stir Welding via Particle Tracing, *International Journal of Metal Forming*,
334 1-15.
- 335 12. Dialami, N., Cervera, M., Chiumenti, M. and Agelet de Saracibar, C. (2016) Local-global strategy for
336 the prediction of residual stresses in FSW processes, *International Journal of Advanced Manufacturing*
337 *Technology*, 1-13.
- 338 13. Dialami, N., Chiumenti, M., Cervera, M. and Agelet de Saracibar, C. (2017) Challenges in
339 thermo-mechanical analysis of Friction Stir Welding processes, *Archives of Computational Methods in*
340 *Engineering*, 24:189-225.
- 341 14. Dialami, N., Chiumenti, M., Cervera, M. and Agelet de Saracibar, C. (2017) A fast and accurate
342 two-stage strategy to evaluate the effect of the pin tool profile on metal flow, torque and forces during
343 friction stir welding, *International Journal of Mechanical Sciences* 122:215-227.
- 344 15. Dialami N., Chiumenti M., Cervera M., Segatori A. and Osikowicz W. (2017) Enhanced friction model
345 for Friction Stir Welding (FSW) analysis: simulation and experimental validation, *International Journal*
346 *of Mechanical Sciences* 133: 555-567.

- 347 16. Ryzhakov P, Rossi R, Oñate E (2011) An algorithm for the simulation of thermally coupled low speed
348 flow problems. *Int J Numer Methods Fluids* 65: 1217–1230.
- 349 17. Ravichandran G., Rosakis A. J., Hodowany J. and Rosakis Ph. (2002) On the Conversion of Plastic
350 Work into Heat During High Strain Rate Deformation *AIP Conference Proceedings* 620, 557
- 351 18. Nandan R., DebRoy T. and Bhadeshia H. K. D. H. (2008) Recent Advances in Friction Stir Welding –
352 Process, Weldment Structure and Properties, *Progress in Materials Science* 53: 980-1023
- 353 19. Chao, Y.J., Qi, X. and Tang, W. (2003), Heat transfer in friction stir welding – experimental and
354 numerical studies, *Journal of Manufacturing Science and Engineering* 125:138-45.
- 355 20. Khandkar, M.Z.H., Khan, J.A., Reynolds, A.P. and Sutton, M.A. (2006), Predicting residual stresses in
356 friction stir welded metals, *Journal of Materials Processing Technology*, 174:195-203.
- 357 21. Serio L, Palumbo D, Galietti U, De Filippis L, Ludovico A. (2016) Effect of Friction Stir Process
358 Parameters on the Mechanical and Thermal Behavior of 5754-H111 Aluminum Plates. *Materials*,
359 9(3):122.
- 360 22. De Filippis L, Serio L, Palumbo D, D Finis R, Galietti U. (2017) Optimization and Characterization of
361 the Friction Stir Welded Sheets of AA 5754-H111: Monitoring of the Quality of Joints with
362 Thermographic Techniques. *Materials*, 10:1165.
- 363 23. Seidel T.U., Reynolds A.P. (2001) Visualization of the material flow in AA2195 friction-stir welds using
364 a marker insert technique. *Metall. Mater. Trans. A* 32, 2879–2884.
- 365 24. Mishra RS, De PS, Kumar N (2014) Fundamentals of the friction stir process. In: *Friction stir welding*
366 and processing. Springer: 13–58.



© 2017 by the authors. Submitted for possible open access publication under the terms and conditions of the Creative Commons Attribution (CC BY) license (<http://creativecommons.org/licenses/by/4.0/>).